RSC Advances

PAPER

Cite this: *RSC Adv.*, 2016, **6**, 30311

First principles study on the structural evolution and properties of $(MCl)_n$ ($n = 1$–12, M = Cu, Ag) clusters

Zhimei Tian[ab] and Longjiu Cheng*[a]

Received 15th January 2016
Accepted 12th March 2016

DOI: 10.1039/c6ra01258b

www.rsc.org/advances

The structural evolution of $(MCl)_n$ (M = Cu, Ag, $n = 1$–12) clusters has been explored using a first principles global minimization technique, namely, a genetic algorithm from density functional theory geometry optimization (GA-DFT). Benchmark calculations indicate that the method used in this work is reliable in predicting the energetic sequences of different isomers of $(CuCl)_6$ clusters compared to the high-level coupled cluster method. The computational results indicate that the structures of $(CuCl)_n$ and $(AgCl)_n$ clusters share many similarities. The global minima of $(MCl)_n$ clusters are planar and nonplanar monocyclic structures up to $n = 5$, and multi-ring or catenane structures when $n \geq 6$. The characters of the intramolecular interactions of $(AgCl)_3$, $(CuCl)_3$, $(CuCl)_4$ and $(CuCl)_6$ clusters have been studied by the noncovalent interactions (NCI) index. The electronic and bonding properties of $(CuCl)_3$ and $(AgCl)_3$ clusters are analyzed. At a higher level, the refined energies of the isomers, the binding energies and the second difference of binding energies are calculated, and are examined as a function of the cluster size. Several promising sizes of higher stability and symmetry have been discovered. In particular, we find that the cluster adopts a new folding manner, tube conformation, at $n = 6$, 9 and 12, where they are more stable than the adjacent clusters; moreover, they are aromatic.

Introduction

The study of coinage metal halide clusters has attracted much attention in experiments[1,2] and computations[3–5] because of their practical uses, such as in catalysis and photography, *etc.* From a more fundamental point of view, the interactions between halide and noble metal atoms are difficult to characterize. The ionic bonding character is less marked than in alkali halide systems and the presence of d electrons of the noble metal makes theoretical investigations much more complicated.[6] The exploration of cluster structure is the first step to understand the properties of bulk material. The group 11 halides are particularly interesting. Relativistic effects are important for group 11 compounds, especially for gold compounds, which can lead to significant changes in chemical properties.[7–10] Closed-shell $d^{10}\cdots d^{10}$ interactions among the coinage metal halide clusters have also attracted considerable interest.[11,12]

The crystal structure of CuCl and AgCl have been synthesized,[13–15] however, the physical and chemical properties of small clusters often exhibit significant differences with bulk phase. The evolution of structures and properties with cluster size is a major challenge for experimental and theoretical study.[16] The structures, bonding of Ag_2X, AgX, AgX_2, and AgX_3 (X = F, Cl, Br, I) in gas-phase have been studied.[17] The structure and bonding in M_nX_n (M = Cu, Ag, Au; X = Br, I; $n = 1$–6), have been reported.[18] The trimer evaporation in silver bromide clusters have been used to study the stability, structural and electronic properties of $(Ag_nBr_p)^{(+)}$ ($n = 6$, $p = n$, $n - 1$) clusters.[19] The trimer formation of AgI has been studied experimentally and theoretically.[20] The structures and properties of $(AgBr)_n$ ($n \leq 6$) have been studied.[16] The molecular and electronic structures of $(AgBr)_n$ ($n = 1$–9) clusters have been investigated.[21] The band structures of AgF, AgCl, and AgBr have been reported.[22] A comparison of structure and stability between M_4X_4 (M = Cu, Ag, Au; X = F, Cl, Br, I) has been performed[23] and similar cyclic structures are obtained. Structure and stability of $(CuCl)_n$ and $(AgCl)_n$ ($n = 1$–6) clusters have been studied.[6] Walsh *et al.* predicted the existence and chemical stability of cuprous fluoride.[24] The ground state structures of $(CuCl)_n$ and $(AgCl)_n$ ($n = 4$–6) in previous calculations were not in consistent with each another.[6,23] The possible nuclear arrangements of $(CuCl)_n$ and $(AgCl)_n$ were guessed in previous computations. Thus, the results from the guessed structures are biased. It is worth mentioning that our initial structures of $(CuCl)_n$ and $(AgCl)_n$ are not guessed, but from the results of genetic algorithm (GA).[25–27] The initial structures of GA are then optimized using DFT method.

As former reports reveal, the $(MX)_3$ cluster is particular stable, however, there only exist interpreting analysis of the

[a]*Department of Chemistry, Anhui University, Hefei, Anhui, 230601, China. E-mail: clj@ustc.edu*

[b]*School of Chemistry and Materials Engineering, Fuyang Teachers College, Fuyang, Anhui, 236037, China*

molecular orbitals and ionization energy of the cluster.[4,6,16] Compounds containing two or more metal atoms separated by a shorter distance than the sum of their covalent radii, termed a metallophilic contact such as aurophilic, cuprophilic and argentophilic contacts, are of great interest in both academia and industry.[28–31] These interactions are found to influence significantly a variety of structural and physical characteristics of gold, silver and copper compounds. Lots of experimental and computational studies have been dedicated to the metallophilic contact phenomenon. The noncovalent interaction (NCI) index[32] is applied to characterize the phenomenon of metallophilic interactions.[11,28,33,34] Clearly, a much better understanding of the electronic structure and interactions within the cuprophilic and argentophilic contacts region is necessary for the $(MX)_3$ cluster.

To the best of our knowledge, there are few reports on $(MCl)_n$ (M = Cu, Ag) clusters with $n > 6$. Here we report a systematic study of the structures and properties of $(MCl)_n$ (M = Cu, Ag, n = 1–12) clusters. The structures of the clusters are obtained; the stability, noncovalent interactions and aromatic properties are calculated and discussed.

Computational details

Computational methods

The structures of $(MCl)_n$ (M = Cu, Ag, n = 1–12) clusters are calculated with the combination of GA and DFT method, which has been successfully applied in the structural predictions of many systems.[26,35–39] GA is a search heuristic that mimics the process of natural selection.[25,40] This heuristic is routinely used to generate useful solutions to optimization and search problems. It uses operators that are analogues of the evolutionary processes of mating (or "cross-over" at the gene level), mutation and natural selection to explore multi-dimensional parameter spaces.[26] The GA belongs to the class of evolutionary algorithms, which is an optimization strategy inspired by the Darwinian evolution. This strategy is routinely used to generate useful solutions to optimization and search problems. Starting with a population of candidate structures, we relax these candidates to the nearest local minimum. Using the relaxed energies as the criteria, a fraction of the population is selected as "parents". The next generation of candidate structures is the structure mating the "parents". The progress is repeated until the global minimum (GM) is located.[25,41] DFT based GA is very time-consuming, and when cluster size $n \geq 2$, more than 1000 samplings are optimized by DFT. The quantum chemical calculations are performed with the Gaussian 09 suite of programs.[42] In the optimization procedure, the Lanl2dz basis set and 6-31G(d) basis set are used for the coinage metals and Cl at TPSSh functional level[43] without any symmetry constraint, and the normal mode frequencies are also computed at the same level for all structures to ensure that they belong to minima. All the minima are verified by the absence of imaginary frequency. The refined energies of the isomers and the binding energies are calculated using the small-core relativistic effective core potentials, ECP10MDF[43] and ECP28MDF[44] for Cu and Ag, respectively, with the corresponding correlation consistent valence basis sets (aVDZ),[44,45] and the aug-cc-pvdz basis set for Cl. Hereafter, the reported energy differences of the isomers are calculated at this level. The ionization potentials of Cu and Ag atoms calculated at this level are 7.80 and 7.67 eV, respectively, which are in consistent with the corresponding experimental values (7.73 and 7.58 eV),[46] indicating that our calculation method is reliable. Noncovalent interaction (NCI) plots are plotted using Multiwfn[47,48] and VMD[49] packages. The nucleus-independent chemical shift (NICS)[50] method has been used to study the aromaticity of partial clusters.

Benchmark calculations

To verify the reliability of the methods used in this work, a benchmark calculation is carried out by comparing the relative stability of the three isomers of $(CuCl)_6$ cluster (see structures in Fig. 1) using different basis sets at CCSD(T) level of theory. Results of the benchmark calculations are given in Table 1. Note that the relative stabilities of **6II** and **6III** are highly overestimated by TPSSh/Lanl2dz and 6-31G(d) method. However, the relative stability of the three isomers obtained by the refined energies at TPSSh level is in overall consistent with the results obtained at the CCSD(T) level. The comparison suggests that the refined energies are necessary and reliable in predicting relative stability of $(CuCl)_6$ cluster.

Results and discussion

The equilibrium geometries of $(CuCl)_n$ and $(AgCl)_n$ with n = 1–12 clusters are plotted in Fig. 1 and 2, respectively. The structures are indexed in Roman number order (I, II, III) and alphabetical order (A, B, C) by the energy from low to high for $(CuCl)_n$ and $(AgCl)_n$ clusters, respectively. The symmetry and relative energies of the isomers are also shown.

Geometric structure

The bond length of **1I** and **1A** are 2.11 and 2.34 Å, respectively, which are both in $C_{\infty v}$ symmetry. The corresponding experimental results are 2.055 and 2.281 Å.[51,52] Both of them are reasonably close to the experimental values.

For dimers, the D_{2h} rhombus is the lowest-energy isomer, namely, **2I** and **2A**. In **2I**, the Cu–Cl and Cu–Cu bond lengths are 2.32 and 2.44 Å, respectively, and a Cu–Cl–Cu angle of 63°. The Ag–Cl and Ag–Ag distances in **2A** are 2.56 and 2.85 Å, respectively, and Ag–Cl–Ag angle of 68°. Our results are in accordance with similar system M_2Br_2, M = Cu, Ag and Au using B3LYP functional.[18]

The trimer (**3I** and **3A**) is a quasi-triangular shape with D_{3h} symmetry and strong M–M interactions favored by relatively short distances (2.65 and 2.99 Å for Cu–Cu and Ag–Ag bond lengths, respectively). **3I** and **3A** consist of halide atoms with metal atoms bridging the Cl–Cl bonds. The Cu–Cl bond lengths in **3I** are all equivalent, 2.24 Å. The Ag–Cl bond lengths in **3A** are also the same, 2.46 Å. In agreement with previous B3LYP and matrix-IR spectra reports of $(AgCl)_3$, our calculations give a planar six-membered ring structure.[20,53] The Cl–Cu–Cl and Cl–Ag–Cl angles in **3I** and **3A** are 167° and 165°, respectively. The

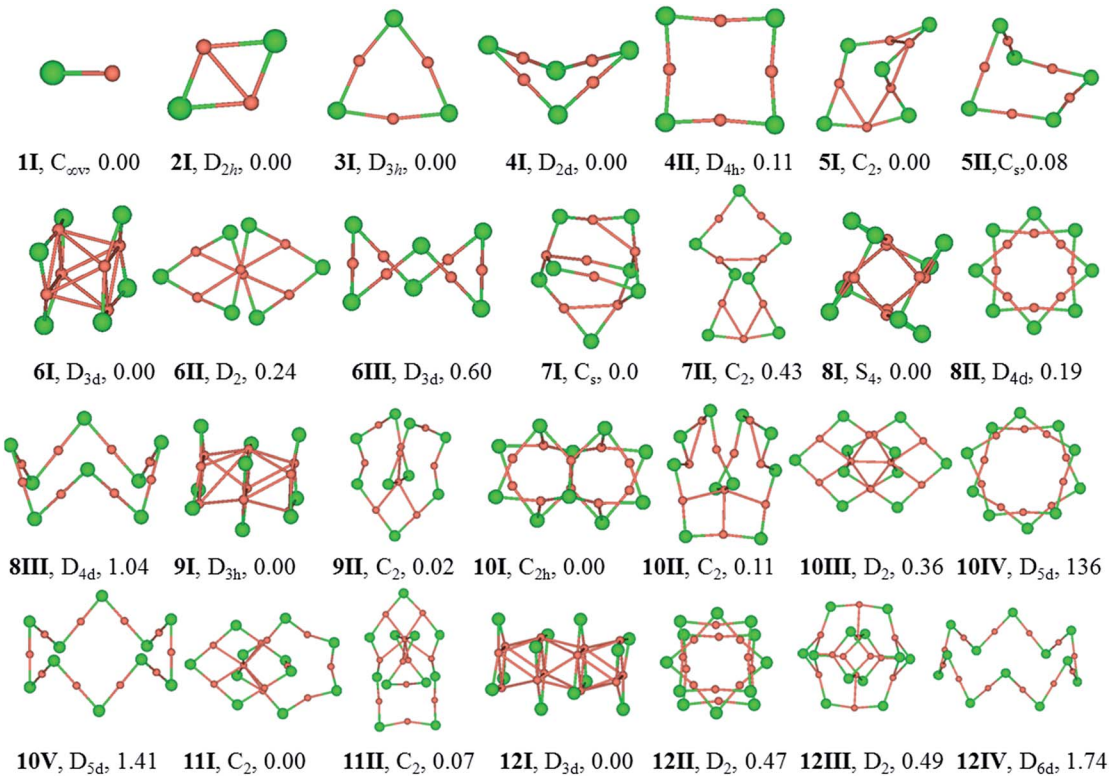

Fig. 1 Optimized structures of low-lying isomers of $(CuCl)_n$ (n = 1–12) at TPSSh/Lanl2dz (Cu) and 6-31G(d) (Cl) level of theory. The numbers under the structures are the relative energies in eV at TPSSh level using aVDZ and aug-cc-pvdz basis sets for Cu (ECP10MDF) and Cl, respectively. The structures labelled in *n*I correspond to the global minima, *n*II–*n*V are local minima that are higher in energy, and the symmetries are labeled in figure. Cu-pink, Cl-green.

Table 1 Comparison of single point energies for the three low-lying isomers of $(CuCl)_6$ (see structures in Fig. 1)[a]

Method	6I	6II	6III
TPSSh/Lanl2dz, 6-31G(d)	−3938.0677611	0.75	1.15
TPSSh[b]	−3945.4014317	0.13	0.46
CCSD(T)/aug-cc-pvdz, aug-cc-pvdz-pp	−3938.4000069	0.02	0.20
CCSD(T)/Lanl2dz	−1260.0751833	0.20	0.15
CCSD(T)/6-311+G(d)	−12 594.0672619	0.23	0.34
CCSD(T)/def2-tzvp	−12 594.8747943	0.11	0.14
CCSD(T)/cc-pvtz	−12 595.7453668	0.03	0.05

[a] Energies for **6I** are in atomic units, while other energies are relative to this in eV. Results are single point energies for TPSSh (Lanl2dz (metal) and 6-31G(d) (Cl)) geometry. [b] Energies are calculated using the relativistic effective core potential ECP10MDF for Cu with the corresponding correlation consistent valence basis sets (aVDZ), and the aug-cc-pvdz basis set for Cl.

Cu–Cl–Cu and Ag–Cl–Ag angles are 73° and 75° in **3I** and **3A**, respectively.

For tetramer, it favors a nonplanar distorted D_{2d} symmetry structure (**4I** and **4A**) with a D_{4h}-symmetry isomer (**4II** and **4B**) 0.11 and 0.05 eV higher in energy for $(CuCl)_4$ and $(AgCl)_4$, respectively. The Cu–Cl and Cu–Cu bond distances in **4I** are 2.21 and 2.76 Å, respectively, and the Cl–Cu–Cl angle is 178°, which indicates that the ClCuCl atoms are almost aligned. The Ag–Cl and Ag–Ag bond distances in **4A** are 2.43 and 3.24 Å, respectively, and the Cl–Ag–Cl angle is 179°. In **4B**, the Ag–Cl and Ag–Ag distances are 2.43 and 3.46 Å, respectively, the Cl–Ag–Cl and Ag–Cl–Ag angles are 179° and 91°, respectively. Our computational results of the stable isomers are in agreement with that of $(CuBr)_4$ cluster.[54]

5I and **5A** are in cyclic arrangement, which are in C_2 and C_s symmetries, respectively. It can be described as a nonplanar distorted pentagon with Cl apexes and ClMCl sides having different M–Cl–M angles (ranging from 71° to 98°) around the cycle. The 10 M–Cl bond lengths are in the range of 2.22–2.27 and 2.43–2.44 Å for Cu–Cl and Ag–Cl, respectively. **5II** is a distorted structure with C_s symmetry, 0.08 eV higher in energy than **5I**. **5B** is a C_s symmetry structure with one chloride atom capping one tetramer ring, 0.39 eV higher in energy than **5A**.

6I and **6A** are both tube structures in D_{3d} symmetry with two quasi-planar triangle units paralleling to each other. The conformation has been revealed in $(AgBr)_6$ cluster.[16] The 12 M–Cl bond lengths are strictly identical in **6I** and **6A**, 2.29 and 2.52 Å for Cu–Cl and Ag–Cl, respectively, and the metal–metal distances are found to be 2.72 and 3.08 Å for Cu–Cu and Ag–Ag in the two triangles of **6I** and **6A**, respectively. **6II** and **6B** are helix structures in D_2 symmetry, lying 0.24 and 0.37 eV higher in energy than **6I** and **6A**, respectively. **6III** and **6C** are the known zigzag crown conformations in D_{3d} symmetry, lying 0.60 and 0.56 eV higher in energy than **6I** and **6A**, respectively.

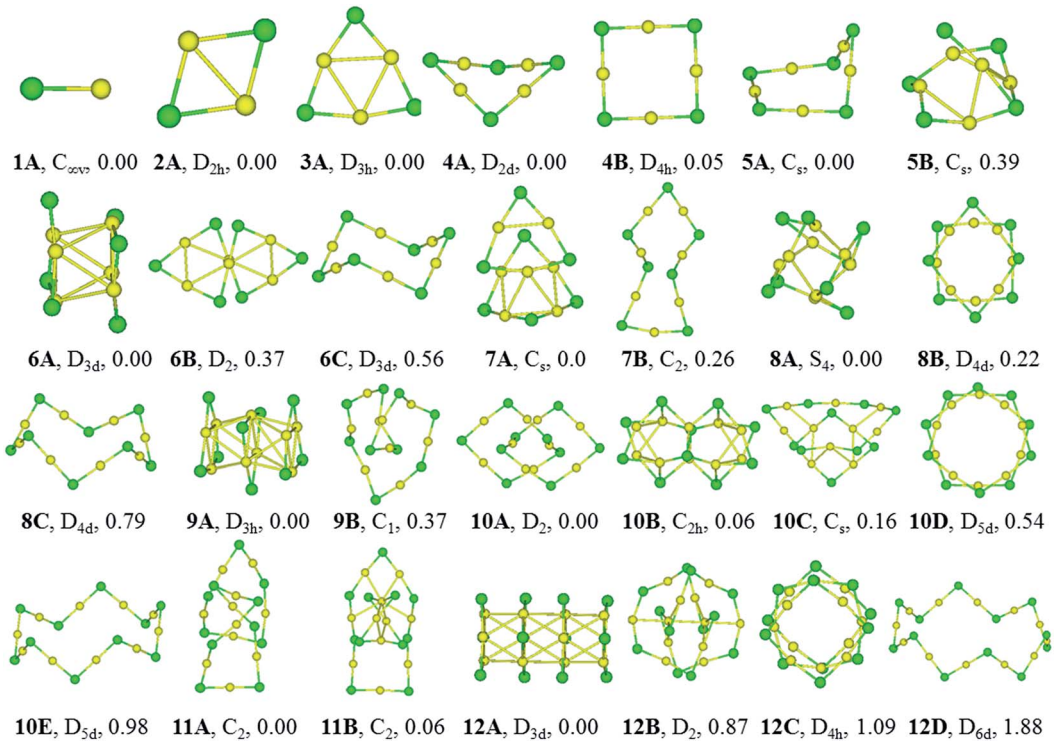

Fig. 2 Optimized structures of low-lying isomers of $(AgCl)_n$ (n = 1–12) at TPSSh/Lanl2dz (Ag) and 6-31G(d) (Cl) level of theory. The numbers under the structures are the relative energies in eV at TPSSh level using aVDZ and aug-cc-pvdz basis sets for Ag (ECP28MDF) and Cl, respectively. The structures labelled in nA correspond to the global minima, nB–nE are local minima that are higher in energy, and the symmetries are labeled in figure. Ag-yellow, Cl-green.

7I and **7A** are distorted structures in C_s symmetry, consisting of one six-member-ring and one eight-member-ring. The Cu–Cl bond lengths are in the range of 2.21–2.58 Å and Cl–Cu–Cl angles are in the range of 103.4–164.1° in **7I**. In **7A**, the Cl–Ag–Cl angle that near the center of the $(AgCl)_4$ part is 157.4°, and much smaller than the two adjacent Cl–Ag–Cl angles (both 166.6°) in the triangle, which perhaps because it helps to stabilize the structure. **7II** and **7B** are monocyclic structure in C_2 symmetry, 0.43 and 0.26 eV higher in energy than **7I** and **7A**, respectively.

8I and **8A** are windmill structures in S_4 symmetry, and both of which are composed of four seven-member-ring and two six-member-ring units. The Cl–M–Cl angles are in the range of 118.4–163.9°. In **8I**, the bond lengths of Cu–Cl are in the range of 2.24–2.42 Å and the Cu···Cu distance is 2.67 Å; in **8A**, the bond lengths of Ag–Cl are in the range of 2.47–2.64 Å and the Ag···Ag distance is 3.03 Å. **8II** and **8B** in D_{4d} symmetry are separate-ring structures including two paralleling tetramer units, 0.19 and 0.22 eV higher than **8I** and **8A**, respectively. **8III** and **8C** are zigzag crown conformations in D_{4d} symmetries, lying 1.04 and 0.79 eV higher in energy than **8I** and **8A**, respectively.

9I and **9A** are both tube structures in D_{3h} symmetry with three triangular units paralleling to each other. It can be viewed as a tube from the center of the triangular units. In **9I** and **9A**, the 12 M–Cl bond lengths are strictly identical in the side triangles, 2.29 and 2.51 Å, and the 6 M–Cl bond lengths are 2.39 and 2.59 Å in the middle triangle; the M–M bond between the triangle units are strictly 2.84 and 3.19 Å, respectively. **9II** and **9B** are helical structures, lying 0.02 and 0.37 eV higher in energy than **9I** and **9A**, respectively.

10I and **10B** are perfect C_{2h} symmetry structures, consisting of intersecting triangular units. **10A** is a catenane structure in D_2 symmetry. Worth noting is that $(AuSR)_{10}$ cluster has been synthesized and characterized as catenane structure.[55] In **10I**, the Cu–Cl bond lengths range from 2.24 to 2.42 Å, and the Cu–Cl–Cu angle in the center of the structure is 81.2°, which deviates the linearity seriously. **10II** is a helix structure, 0.11 eV higher in energy than **10I**. **10III** is a catenane structure, lying 0.36 eV higher than **10I**. **10C** is a C_s structure consisting of two rings inserting into each other. **10IV** and **10D** are separate-ring structures consisting of two pentamer units. **10V** and **10E** are crown structures in D_{5d} symmetries, 1.41 and 0.98 eV higher in energy than **10I** and **10A**, respectively.

11I and **11A** are catenane structures in C_2 symmetry, with interlocked hexamer and pentamer rings. The Cu–Cl bond lengths in **11I** are in the range of 2.21–2.34 Å, and Cl–Cu–Cl angles are in the range of 148.9–174.3°. The Ag–Cl bond lengths in **11A** are in the range of 2.43–2.56 Å, and ClAgCl angles range from 160.2 to 178.5°. **11II** and **11B** compete with **11I** and **11A** only 0.07 and 0.06 eV higher in energy, respectively, with a tetramer inserting into a heptamer.

12I and **12A** are both tube structures in D_{3d} symmetry, including four paralleling triangle units. The Cu–Cl bond lengths in the side triangles are 2.29 Å and those in the middle

triangles are 2.39 Å, and Cu–Cu bonds are in the range of 2.81–2.87 Å in **12I**. The Ag–Cl bond lengths are strictly identical in the side triangles (2.51 Å), whereas those in the two middle triangles are all 2.59 Å in **12A**. **12II** and **12B** are 0.47 and 0.87 eV higher in energy than **12I** and **12A**, respectively. **12II** and **12C** are both separate ring structures in D_{4h} symmetry, including three tetramer ring units. **12III** is a three-dimensional structure and **12B** is a catenane structure. **12IV** and **12D** are zigzag crown D_{6d} structures, lying 1.74 and 1.88 eV higher in energy than **12I** and **12A**, respectively.

The stable structures in the literatures are all included in our results of GA. The $(MCl)_n$ clusters are planar or nonplanar cycles up to $n = 5$, which is in consistent with similar system $(AgBr)_n$.[19] In this work, the D_{3d} $(AgCl)_6$ isomer is the GM, whereas that of a zigzag crown C_{3v} symmetry structure cluster is the GM of $(AgBr)_6$. The zigzag structure in our work converges to the D_{3d} isomer.[19] Moreover, our results are in agreement with more recent work about $(MBr)_4$ (M = Cu, Ag and Au).[18] The most stable isomers of $(AgCl)_5$ and $(AgCl)_6$ are in C_s and D_{3d} symmetries, which are different from those of $(AgF)_5$ and $(AgF)_6$ whose lowest-energy isomers are in D_{5h} and D_{6h} symmetries.[2] The reason for this is probably due to the strong ionic bond characterization between fluorine and silver atoms. The $(AgF)_n$ are planar cycles up to $n = 6$, whereas the $(MCl)_n$ (M = Cu and Ag) systems can keep planar or non-planar cycles only up to $n = 5$, which suggests that the halogen might be responsible for the tendency to become non-planar.[4] The structural patterns of $(CuCl)_n$ and $(AgCl)_n$ clusters are in consistent with that of $(AuCl)_n$ clusters when $n = 1$–5, however, they are significantly different from $(AuCl)_n$ clusters when $n > 5$ due to the strong aurophilicity of Au element.[56]

Stability

Binding energy. To investigate the stability of the clusters, we calculated the binding energies for $(CuCl)_n$ and $(AgCl)_n$ clusters. Binding energy is defined as $E_b = [n \times E_M + n \times E_{Cl} - E_{(MCl)_n}]/n$ (M = Cu and Ag), where E_b is the total binding energy divided by n. Therefore, E_b is the average binding energy per MCl unit. It is clearly seen that E_b increases as n. Fig. 3a displays the binding energies for $(CuCl)_n$ and $(AgCl)_n$ clusters as a function of cluster size n. From the figure, the binding energies of the $(CuCl)_n$ clusters are bigger than those of the $(AgCl)_n$ clusters. E_b increases quickly up to the trimer and then levels off to pentamer when n ranges from 1 to 5 for $(MCl)_n$, thus the trimer is more stable than the neighboring clusters. This trends in binding energies are similar to that of $(AgBr)_n$ clusters.[21]

The stability of these clusters is also established by the energetic gaps $(E - E_{fit})$ of the GMs, where E is the total energy and E_{fit} is a four-parameter fit of the GM, respectively. The relative stability of the clusters is further assessed with the second difference of binding energies from the following formula: $\Delta_2 E_b(n) = E_b(n+1) + E_b(n-1) - 2E_b(n)$, where E_b is the total binding energy divided by n. The second difference of binding energies is previously used to predict the relative stability of other clusters.[57,58] $E - E_{fit}$ and $\Delta_2 E(n)$ are calculated in a manner that emphasizes particular stable minima or

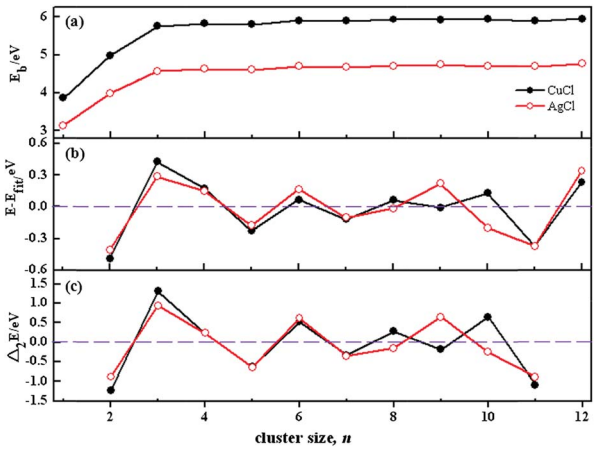

Fig. 3 (a) Binding energies for $(CuCl)_n$ and $(AgCl)_n$ clusters as a function of cluster size n; (b) plot of the energetic gaps $(E - E_{fit})$ of the GMs for $(CuCl)_n$ and $(AgCl)_n$ clusters as a function of cluster size n, where E is the total energy, and E_{fit} is a four-parameter fit of the GMs. $(CuCl)_n$ clusters: $E_{fit} = 3.57471 + 1.17587 \times n^{1/3} - 0.40799 \times n^{2/3} + 0.05064 \times n$, $(AgCl)_n$ clusters: $E_{fit} = 3.57466 + 1.17591 \times n^{1/3} - 0.40800 \times n^{2/3} + 0.05063 \times n$; (c) second difference of binding energies for $(CuCl)_n$ and $(AgCl)_n$ clusters as a function of cluster size n.

"magic numbers" of the clusters. In such curves, positive peaks correspond to more stable structures. The plots of $E - E_{fit}$ and $\Delta_2 E(n)$ as a function of cluster size are shown in Fig. 3b and c, respectively. It can be clearly seen from the figures that, distinctive peaks present at cluster sizes 3, 6, 9 and 12 for $(AgCl)_n$ clusters, indicating their higher relative stability than their neighbours. However, there are distinctive peaks at cluster sizes 3, 6, 8, 10 and 12 of $(CuCl)_n$ clusters. The reasons for the stability difference between $(CuCl)_n$ and $(AgCl)_n$ clusters may be that the GMs at $n = 10$ are different from each other. The particular stability of $(AgCl)_3$ is in agreement with that of $(AgBr)_3$, which is previously reported experimentally and theoretically.[1,3,21]

NCI analysis. From the above analysis, we can see that the $(AgCl)_3$ and $(CuCl)_3$ units are particularly stable. The stability can be analyzed by means of a non-covalent interaction (NCI) map by plotting the reduced density gradient (RDG) *versus* sign $(\lambda_2)\rho$, based on the method proposed by Yang and co-authors.[32,59] Ever since the introduction of NCI analysis, the method has been used to study a number of systems.[28,60–62] NCI involves the reduced density gradient (RDG) and the electron density (ρ). RDG is defined as:

$$s = \frac{1}{2(3\pi^2)^{1/3}} \frac{|\nabla\rho|}{\rho^{4/3}},$$

and the representation of s *versus* ρ shows characteristic peaks at low density values in the presence of noncovalent interactions. The sign of the second eigenvalue (λ_2) of the electron-density Hessian matrix is used to distinguish between bonded $(\lambda_2 < 0)$ and non-bonded $(\lambda_2 > 0)$ interactions. Since the sign of the second eigenvalue sign (λ_2) is indicative for the type of interaction, the analysis results are shown in scatter plots of the reduced density gradient (s) *versus* the electron density (ρ)

multiplied by the sign of λ_2. The spikes in low-density, low-gradient regions in the plots of *s versus* sign $(\lambda_2)\rho$ exhibit the noncovalent interactions. The visualization of the gradient isosurface can be seen in real space through VMD program.[49] The gradient isosurfaces are colored according to the corresponding values of sign $(\lambda_2)\rho$, which is found to be a good indicator of interaction strength.[32] A RGB (red-blue-green) scale is used.

The NCI analysis for $(AgCl)_3$, $(CuCl)_3$, $(CuCl)_4$ and $(CuCl)_6$ clusters is depicted in Fig. 4. Several regions of intramonomer interactions can be distinguished. Favourable (attractive bonding) interactions appear on the left, while unfavourable (nonbonding) on the right. The strength of the NCI is proportional to the density on the NCI surface. Fig. 4a shows the bicolored isosurfaces of $(AgCl)_3$ and $(CuCl)_3$ clusters. The weakening of the metal–metal interaction on going from Cu to Ag (Fig. 4a) can be simply monitored thanks to the shift of the characteristic peak towards more negative values in the NCI plot. The results in Fig. 4a reveal that one strong attractive spike (−0.023 a.u.) is clearly associated to the Ag···Ag interactions in $(AgCl)_3$, whereas two strong steric repulsive spikes (0.016 and 0.023 a.u. of sign $(\lambda_2)\rho$) located at the center and near the M–M bonds of $(AgCl)_3$ cluster. Similarly, there are one attractive spike (−0.029 a.u.) associated to Cu···Cu interactions, and two repulsive spikes (0.025 and 0.029 a.u. of sign $(\lambda_2)\rho$) for $(CuCl)_3$. The attractive and repulsive interactions are clearly stronger than those in $(AgCl)_3$ according the values of sign $(\lambda_2)\rho$. The isosurfaces of $(CuCl)_3$ and $(AgCl)_3$ in the right part of Fig. 4a reveal that the attractive interactions are in blue, whereas the repulsive interactions are in red. It is worth mentioning that the Cu···Cu interactions in $(CuCl)_3$ is stronger than the H bond in water dimer (−0.025 a.u.).[32]

The NCI analysis and isosurface (Fig. 4b) of $(CuCl)_4$ cluster are used to demonstrate the particular stability of $(CuCl)_3$. From the figure, there is one attractive spike (−0.023 a.u.) and two repulsive spikes (0.008 and 0.024 a.u.) in $(CuCl)_4$ cluster. Obviously, the interactions of $(CuCl)_3$ cluster are much stronger than those of $(CuCl)_4$ cluster, indicating $(CuCl)_3$ is more stable than $(CuCl)_4$ cluster, which is in agreement with the stability predicted by binding energy analysis. Moreover, there is a signature of the attractive attraction between the Cu atoms in $(CuCl)_3$ and $(CuCl)_4$ clusters, which could be inferred from the range of the Cu···Cu contacts in them. The distance of Cu···Cu contacts in them are 2.65 and 2.76 Å, respectively, and both of which are smaller than the sum of their van der Waals radii (*ca.* 2.80 Å).[63] It is evident that the distance of Cu···Cu contacts in $(CuCl)_3$ cluster is smaller than that of $(CuCl)_4$, which gives extra support to the NCI analysis.

The Ag/Cl interactions in $(AgCl)_6$ cluster is characterized by a blue region in the isosurface, indicating an attractive interaction. Importantly, the NCI method reveals that the lengthening of the Cu···Cu distance from $(CuCl)_3$ (2.65 Å) to $(CuCl)_6$ (2.72 Å) is accompanied by the weakening of the Cu···Cu interactions. This is manifested in the Fig. 4a and c plots as the shift of the characteristic Cu···Cu peak towards more positive values, namely, changing from 0.029 to 0.026 a.u. Fig. 4c shows the characteristic feature of three spikes in the densities ranging from −0.024 to −0.027 a.u., demonstrating the

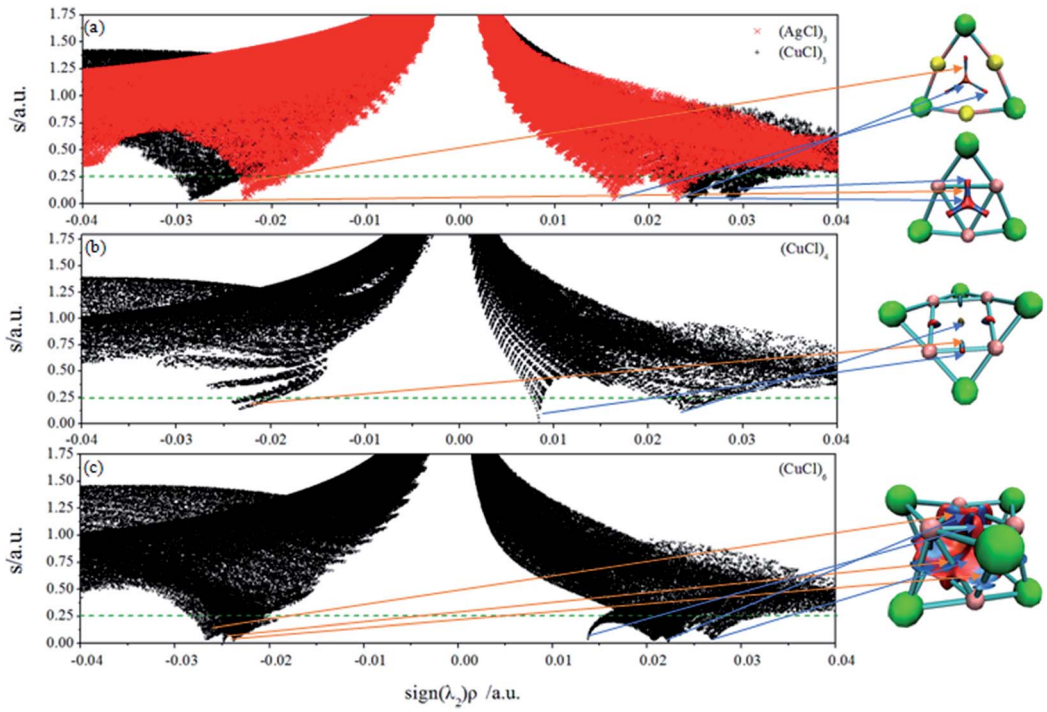

Fig. 4 Plots of the reduced density gradient *versus* the electron density ρ multiplied by the sign of the second Hessian eigenvalue sign (λ_2) (left) and NCI isosurfaces using a blue-green-red colour scale at $s = 0.25$ for the global minim structures (right) of (a) $(AgCl)_3$ and $(CuCl)_3$, (b) $(CuCl)_4$ and (c) $(CuCl)_6$ clusters, respectively. Results were obtained on a cuboid grid using the density and gradient values at the TPSSh/Lanl2dz/6-31G(d) level of theory. Ag-yellow, Cu-pink, Cl-green.

occurrence of attractive noncovalent attractions, and three spikes in the densities changing from 0.014 to 0.027 a.u. manifesting three repulsive interactions. Three kinds of noncovalent interactions of the Cu···Cu interactions in the same $(CuCl)_3$ unit, and Cu···Cu and Cu···Cl interactions between the two $(CuCl)_3$ units are the blue regions of the $(CuCl)_6$ isosurface. The red regions in the isosurface of $(CuCl)_6$ manifest the steric and coulombic repulsion. The stability of $(CuCl)_6$ indicates that the attractive dispersion interactions of Cu···Cu and Cu···Cl contacts outweigh the steric and coulombic repulsion.

Electronic and bonding properties of $(CuCl)_3$ and $(AgCl)_3$ clusters

The most relevant valence molecular orbitals of $(CuCl)_3$ and $(AgCl)_3$ clusters are shown in Fig. 5. Perusal of Fig. 5 reveals that all three-membered copper and silver rings exhibit a composite bonding mode. The bonding of $(CuCl)_3$ and $(AgCl)_3$ clusters is characterized by a common ring-shaped electron density, more commonly seen in organic molecules, which is constructed by highly delocalized σ- and π-type MOs. The delocalized σ and π electron density in the rings could be associated with the cyclic delocalization of electron density, which is a characteristic feature of aromaticity. Interestingly, in the peripheral three-membered rings there are both σ- and π-type MOs (HOMO-15, HOMO-23 for $(CuCl)_3$ cluster, and HOMO-20, HOMO-27 for $(AgCl)_3$ cluster) resulting from the bonding combination of the 3d atomic orbitals (AO) of Cu and 4d AOs of Ag atoms in the rings with the 3p AOs of Cl atoms, respectively. The electronic structure and bonding properties of the three-membered Cu and Ag rings closely resemble those of the aromatic Au rings in Au_3Cl_3 cluster.[64]

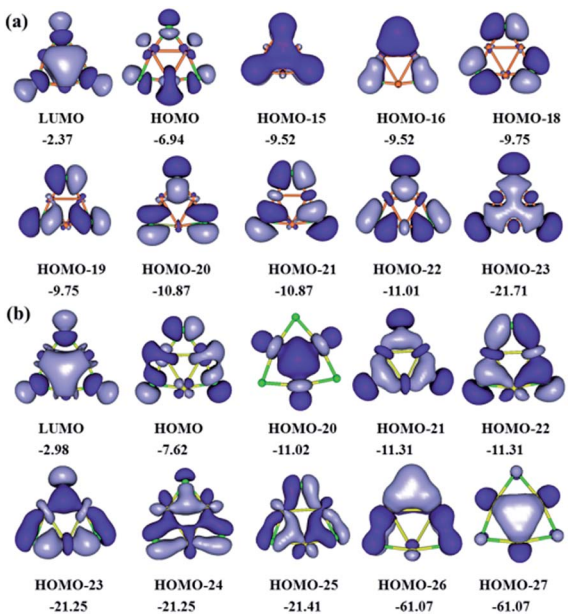

Fig. 5 Most relevant valence molecular orbitals of (a) $(CuCl)_3$ and (b) $(AgCl)_3$ clusters (isocontour value of 0.02 a.u.; eigenvalues in eV).

Aromaticity

Planarity, high stability, bond length equalization, and HOMO–LUMO gaps are conventionally good indicators of aromaticity.[65] Nucleus-independent chemical shift (NICS) value[50] is the most widely used as a quantitative measure for aromaticity. Negative NICS values indicate aromaticity, while positive values imply antiaromaticity. NICS values are the negative of absolute magnetic shielding tensors. In 2001, Boldyrev *et al.* reported the experimental and theoretical evidence of aromaticity in Al_4^{2-}, an all-metal compound.[66] Tsipis *et al.* have investigated the aromatic properties in gold and silver rings of M_nH_n (M = Ag, Au; $n = 3$–6) molecules and the ligand-stabilized aromatic three-membered gold rings in a series of cyclo-$Au_3L_nH_{3-n}$ (L = CH_3, NH_2, OH and Cl; n = 1–3).[64,65] The DFT study of "all-metal" aromatic compounds has been reviewed by Tsipis.[67] All-metal aromaticity and antiaromaticity, and the aromaticity in transition-metal systems have been reported.[68,69] Stanger introduced the NICS-scan method,[70] which is analogous to the aromatic ring center shieldings approach. Here, we employ NICS-scan method to analyze the aromaticity of the tube clusters. Considering that the out-of-plane component of NICS-scan, NICSzz-scan, is a better index of aromaticity,[71,72] the aromatic properties along z-axes (coined as NICSzz-scan) within the range of −4.0–4.0 Å above the geometric centers of the clusters are calculated. NICS(0) positions of NICSzz-scan curves are the geometric centers of the clusters. Fig. 6 plots the NICSzz-scan curves for $(AgCl)_3$, $(CuCl)_3$, $(CuCl)_6$ and $(CuCl)_9$ clusters. It can be seen that all the molecules exhibit negative NICS(0) values, and the NICS values obtained at various positions inside, above or outside the molecular frame proved the existence of diatropic ring-current effect, characteristic for aromaticity. Based on the figure, $(AgCl)_3$ cluster is generally less aromatic than $(CuCl)_n$ clusters. Noteworthy is that the NICS(0) value of $(AgCl)_3$ (−11.3 ppm) is smaller than that of $(CuCl)_3$ (−14.6 ppm), and both of which are smaller than the that of Au_3Cl_3 cluster (−23.8 ppm).[64] From the figure, we can see that the curves oscillate. Concretely, there is one trough of wave in

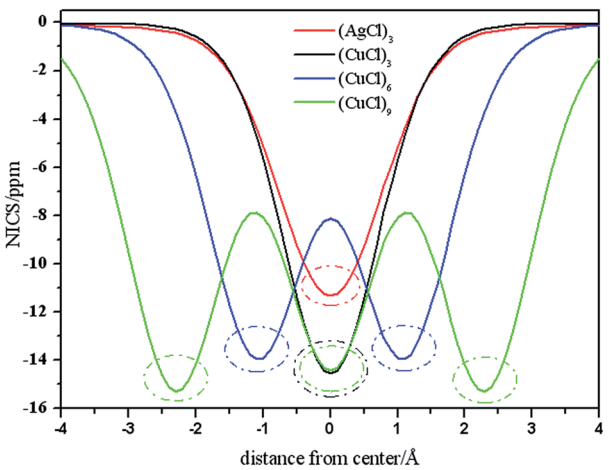

Fig. 6 The NICSzz-scan curves for $(AgCl)_3$, $(CuCl)_3$, $(CuCl)_6$, $(CuCl)_9$ and $(CuCl)_{12}$ within the range of −4.0 to 4.0 Å above the geometric centers of the clusters.

the NICSzz-scan curves (red and black curves) of $(AgCl)_3$ and $(CuCl)_3$ clusters, respectively. There are two and three troughs of wave in the NICSzz-scan curves (blue and green curves) of $(CuCl)_6$ and $(CuCl)_9$ clusters, respectively. Analysis of the data obtained, it is obviously that the aromaticity of the center of the $(MCl)_3$ unit is higher than the neighboring positions along *z*-axis of the cluster. It is concluded that the curves oscillate due to the $(MCl)_3$ unit. In Fig. 6, the $(MCl)_3$ units displayed in dotted oval, and the aromaticity brought by the $(MCl)_3$ unit can be clearly seen. The NICS-scan curves of $(CuCl)_3$, $(CuCl)_6$ and $(CuCl)_9$ clusters exhibit one, two and three dotted ovals, respectively. In a word, the $(MCl)_3$ unit can be proved existing based on NICS-scan method.

Conclusions

In present work, the geometries of $(MCl)_n$ ($n = 1$–12, M = Cu and Ag) clusters are investigated using the method combining GA with TPSSh functional. The relevant low-lying structures are obtained. The computational results indicate that the structures of $(CuCl)_n$ and $(AgCl)_n$ clusters share many similarities. The global minima structures are planar and nonplanar cyclic structures in the range of $n = 1$–5. At $n = 7$, a distorted low symmetric structure is the most stable isomer. At $n = 8$, the windmill structure is the global minimum. When $n = 3$, 6, 9 and 12, $(AgCl)_n$ clusters are more stable than neighboring clusters, whereas $(CuCl)_n$ clusters are more stable than neighboring clusters at $n = 3$, 6, 8, 10 and 12. The four three-member-ring structure intersecting cubic structure is the most stable isomer for $(CuCl)_{10}$, whereas the catenane isomer is most stable for $(AgCl)_{10}$ cluster. The trimer is very stable with high binding energy. A new folding manner, tube conformation, is found for $(CuCl)_n$ and $(AgCl)_n$ clusters. When *n* is the integral multiple of three and the structure includes triangular units, it exhibits aromatic. The NICS-scan method and NCI index are used to character the clusters.

Acknowledgements

This work is supported by the National Natural Science Foundation of China (21273008, 21573001), the Natural Science Foundation of Anhui Provincial University (2015KJ013) and the financial support of the Fuyang Teachers College (2015FSKJ12). The calculations are carried out on the High-Performance Computing Centre of Anhui University.

References

1 J. M. L'Hermite, F. Rabilloud, P. Labastie and F. Spiegelman, *Eur. Phys. J. D*, 2001, **16**, 77–80.
2 F. Rabilloud, O. Bonhomme, J. M. L'Hermite and P. Labastie, *Chem. Phys. Lett.*, 2008, **454**, 153–157.
3 P. Koirala, M. Willis, B. Kiran, A. K. Kandalam and P. Jena, *J. Phys. Chem. C*, 2010, **114**, 16018–16024.
4 F. Rabilloud and D. Mathian, *J. Cluster Sci.*, 2012, **23**, 165–176.
5 Q. Wang, Q. Sun and P. Jena, *J. Chem. Phys.*, 2009, **131**, 124301.
6 F. Rabilloud, *J. Comput. Chem.*, 2012, **33**, 2083–2091.
7 N. Shao, Y. Pei, Y. Gao and X. C. Zeng, *J. Phys. Chem. A*, 2009, **113**, 629–632.
8 H. Grönbeck, M. Walter and H. Häkkinen, *J. Am. Chem. Soc.*, 2006, **128**, 10268–10275.
9 L. Cheng, Y. Yuan, X. Zhang and J. Yang, *Angew. Chem., Int. Ed.*, 2013, **52**, 9035–9039.
10 Y. Yuan, L. Cheng and J. Yang, *J. Phys. Chem. C*, 2013, **117**, 13276–13282.
11 J. M. López de Luzuriaga, M. Monge, M. E. Olmos and D. Pascual, *Organometallics*, 2015, **34**, 3029–3038.
12 G. R. Desiraju, *J. Chem. Soc., Dalton Trans.*, 2000, 3745–3751.
13 A. Taubert, *Angew. Chem.*, 2004, **116**, 5494–5496.
14 M. C. Li, H. Yu, R. Huang, F. Bai, M. Trevor, D. D. Song, B. Jiang and Y. F. Li, *Nanoscale Res. Lett.*, 2013, **8**, 1–6.
15 H. Daupor and S. Wongnawa, *Mater. Chem. Phys.*, 2015, **159**, 71–82.
16 Y. H. Yin, H. S. Chen and Y. Song, *J. Mol. Struct.: THEOCHEM*, 2010, **959**, 30–34.
17 H. C. Müller Rösing, A. Schulz and M. Hargittai, *J. Am. Chem. Soc.*, 2005, **127**, 8133–8145.
18 F. Rabilloud, *J. Phys. Chem. A*, 2012, **116**, 3474–3480.
19 F. Rabilloud, F. Spiegelman, J. L'Hermite and P. Labastie, *J. Chem. Phys.*, 2001, **114**, 289–305.
20 A. Kovács and R. J. Konings, *J. Mol. Struct.*, 2002, **643**, 155–160.
21 H. Zhang and Z. Schelly, *J. Phys. Chem. A*, 2000, **104**, 6287–6294.
22 S. Glaus and G. Calzaferri, *Photochem. Photobiol. Sci.*, 2003, **2**, 398–401.
23 P. Schwerdtfeger, R. P. Krawczyk, A. Hammerl and R. Brown, *Inorg. Chem.*, 2004, **43**, 6707–6716.
24 A. Walsh, C. R. A. Catlow, R. Galvelis, D. O. Scanlon, F. Schiffmann, A. A. Sokol and S. M. Woodley, *Chem. Sci.*, 2012, **3**, 2565–2569.
25 D. M. Deaven and K. M. Ho, *Phys. Rev. Lett.*, 1995, **75**, 288–291.
26 R. L. Johnston, *Dalton Trans.*, 2003, 4193–4207.
27 A. Shayeghi, D. Götz, J. Davis, R. Schaefer and R. L. Johnston, *Phys. Chem. Chem. Phys.*, 2015, **17**, 2104–2112.
28 B. Pinter, L. Broeckaert, J. Turek, A. Růžička and F. De Proft, *Chem.–Eur. J.*, 2014, **20**, 734–744.
29 A. Chakraborty, K. K. Ramachandran, S. S. Yamijala, S. K. Pati and T. K. Maji, *RSC Adv.*, 2014, **4**, 35167–35170.
30 M. Hapka, M. Dranka, K. Orłowska, G. Chałasiński, M. M. Szczęśniak and J. Zachara, *Dalton Trans.*, 2015, **44**, 13641–13650.
31 H. Schmidbaur and A. Schier, *Angew. Chem., Int. Ed.*, 2015, **54**, 746–784.
32 E. R. Johnson, S. Keinan, P. Mori Sanchez, J. Contreras Garcia, A. J. Cohen and W. T. Yang, *J. Am. Chem. Soc.*, 2010, **132**, 6498–6506.
33 H. L. Hermann, G. Boche and P. Schwerdtfeger, *Chem.–Eur. J.*, 2001, **7**, 5333–5342.

34 E. Wächtler, S. H. Privér, J. R. Wagler, T. Heine, L. Zhechkov, M. A. Bennett and S. K. Bhargava, *Inorg. Chem.*, 2015, **54**, 6947–6957.

35 L. Ren, L. J. Cheng, Y. Feng and X. M. Wang, *J. Chem. Phys.*, 2012, **137**, 014309.

36 L. J. Cheng and J. L. Yang, *J. Chem. Phys.*, 2013, **138**, 141101.

37 L. F. Li and L. J. Cheng, *J. Chem. Phys.*, 2013, **138**, 094312.

38 Y. Yuan and L. Cheng, *J. Chem. Phys.*, 2012, **137**, 044308.

39 Z. M. Tian and L. J. Cheng, *Phys. Chem. Chem. Phys.*, 2015, **17**, 13421–13428.

40 R. Ferrando, J. Jellinek and R. L. Johnston, *Chem. Rev.*, 2008, **108**, 845–910.

41 S. Hamad, C. Catlow, S. Woodley, S. Lago and J. Mejias, *J. Phys. Chem. B*, 2005, **109**, 15741–15748.

42 M. J. Frisch, H. B. Schlegel, G. E. Scuseria, M. A. Robb, J. R. Cheeseman, G. Scalmani, V. Barone, B. Mennucci, G. A. Petersson, H. Nakatsuji, M. Caricato, X. Li, H. P. Hratchian, A. F. Izmaylov, J. Bloino, G. Zheng, J. L. Sonnenberg, M. Hada, M. Ehara, K. Toyota, R. Fukuda, J. Hasegawa, M. Ishida, T. Nakajima, Y. Honda, O. Kitao, H. Nakai, T. Vreven, J. A. Montgomery, J. E. P. Peralta, F. Ogliaro, M. Bearpark, J. J. Heyd, E. Brothers, K. N. Kudin, V. N. Staroverov, T. Keith, R. Kobayashi, J. Normand, K. Raghavachari, A. Rendell, J. C. Burant, S. S. Iyengar, J. Tomasi, M. Cossi, N. Rega, J. M. Millam, M. Klene, J. E. Knox, J. B. Cross, V. Bakken, C. Adamo, J. Jaramillo, R. Gomperts, R. E. Stratmann, O. Yazyev, A. J. Austin, R. Cammi, C. Pomelli, J. W. Ochterski, R. L. Martin, K. Morokuma, V. G. Zakrzewski, G. A. Voth, P. Salvador, J. J. Dannenberg, S. Dapprich, A. D. Daniels, O. Farkas, J. B. Foresman, J. V. Ortiz, J. Cioslowski and D. J. Fox, *Gaussian 09, revision B. 01*, Gaussian, Inc., Wallingford, CT, 2009.

43 J. Tao, J. P. Perdew, V. N. Staroverov and G. E. Scuseria, *Phys. Rev. Lett.*, 2003, **91**, 146401.

44 D. Figgen, G. Rauhut, M. Dolg and H. Stoll, *Chem. Phys.*, 2005, **311**, 227–244.

45 K. A. Peterson and C. Puzzarini, *Theor. Chem. Acc.*, 2005, **114**, 283–296.

46 J. Sugar and A. Musgrove, *J. Phys. Chem. Ref. Data*, 1990, **19**, 527–616.

47 H. P. Loock, L. M. Beaty and B. Simard, *Phys. Rev. A*, 1999, **59**, 873.

48 T. Lu and F. W. Chen, *J. Comput. Chem.*, 2012, **33**, 580–592.

49 W. Humphrey, A. Dalke and K. Schulten, *J. Mol. Graphics*, 1996, **14**, 33–38.

50 P. V. R. Schleyer, C. Maerker, A. Dransfeld, H. Jiao and N. J. V. E. Hommes, *J. Am. Chem. Soc.*, 1996, **118**, 6317–6318.

51 K. P. Huber and G. Herzberg, *Constants of diatomic molecules*, Springer, 1979.

52 F. H. de Leluw and A. Dymanus, *J. Mol. Spectrosc.*, 1973, **48**, 427–445.

53 T. Martin and H. Schaber, *J. Chem. Phys.*, 1980, **73**, 3541–3546.

54 K. A. Kacprzak, O. Lopez-Acevedo, H. Häkkinen and H. Gronbeck, *J. Phys. Chem. C*, 2010, **114**, 13571–13576.

55 M. R. Wiseman, P. A. Marsh, P. T. Bishop, B. J. Brisdon and M. F. Mahon, *J. Am. Chem. Soc.*, 2000, **122**, 12598–12599.

56 Y. Liu, Z. M. Tian and L. J. Cheng, *RSC Adv.*, 2016, **6**, 4705–4712.

57 C. Priest, Q. Tang and D. E. Jiang, *J. Phys. Chem. A*, 2015, **119**, 8892–8897.

58 S. Darby, T. V. Mortimer-Jones, R. L. Johnston and C. Roberts, *J. Chem. Phys.*, 2002, **116**, 1536–1550.

59 J. Contreras García, E. R. Johnson, S. Keinan, R. Chaudret, J. P. Piquemal, D. N. Beratan and W. T. Yang, *J. Chem. Theory Comput.*, 2011, **7**, 625–632.

60 L. López, P. Ruiz, M. Castro, J. Quijano, M. Duque-Noreña, P. Pérez and E. Chamorro, *RSC Adv.*, 2015, **5**, 62946–62956.

61 J. Soto-Delgado, J. Torras, L. J. del Valle, F. Estrany and C. Alemán, *RSC Adv.*, 2015, **5**, 9189–9203.

62 Y. Q. Feng and L. J. Cheng, *RSC Adv.*, 2015, **5**, 62543–62550.

63 A. Bondi, *J. Phys. Chem.*, 1964, **68**, 441–451.

64 A. C. Tsipis and C. A. Tsipis, *J. Am. Chem. Soc.*, 2005, **127**, 10623–10638.

65 C. A. Tsipis, E. E. Karagiannis, P. F. Kladou and A. C. Tsipis, *J. Am. Chem. Soc.*, 2004, **126**, 12916–12929.

66 X. Li, A. E. Kuznetsov, H. F. Zhang, A. I. Boldyrev and L. S. Wang, *Science*, 2001, **291**, 859.

67 C. A. Tsipis, *Coord. Chem. Rev.*, 2005, **249**, 2740–2762.

68 A. I. Boldyrev and L. S. Wang, *Chem. Rev.*, 2005, **105**, 3716.

69 T. R. Galeev and A. I. Boldyrev, *Annu. Rep. Prog. Chem., Sect. C: Phys. Chem.*, 2011, **107**, 124–147.

70 A. Stanger, *J. Org. Chem.*, 2006, **71**, 883–893.

71 P. V. R. Schleyer, M. Manoharan, H. Jiao and F. Stahl, *Org. Lett.*, 2001, **3**, 3643–3646.

72 C. Corminboeuf, T. Heine, G. Seifert, P. von Ragué Schleyer and J. Weber, *Phys. Chem. Chem. Phys.*, 2004, **6**, 273–276.